Supporting information

Experimental

$LiBH_4$ (Acros, 95.0 %) $NaBH_4$ (Aldrich, 98.0 %), and $FeCl_3$ (Alfa Aesar, 98.0 %) were used without further purification. The borohydride hydrazinate complexes were synthesized by ball-milling borohydride and hydrazine in a certain ratio on a Retsch PM 400 planetary mill at 150 rpm under an inert atmosphere for 2h. The ball-to-sample weight ratio was about 30:1. We denote samples by $M(BH_4)_n \bullet xNH_2NH_2$, where x means the molar ratio of hydrazine to borohydride. Fe precursor ($FeCl_3$) was introduced into samples through ball milling at 150 ppm for 5h. To reduce the heat effect in milling, the mill was set to revolve for 2 min in one direction and pause 15 s, and then revolve in reversal direction. All the material handlings were performed inside an MBraun glovebox filled with purified argon. XRD characterizations were conducted on a PANalytical X'pert diffractometer (Cu Kα, 40kV, 40mA). To avoid sample contamination by air, the sample was sealed in a home-made sample holder covered by a piece of shielding film. Volumetric release measurements were performed on a home-made Sievert type apparatus to quantify the gas evolution. The gaseous products were introduced into a diluted sulphuric acid to detect NH_3 concentration from the change of conductivity of the acid solution described elsewhere[S1]. XAFS and high-resolution XRD spectra were collected at BL14W1 beamline and BL14B1 beamline of Shanghai Synchrotron Radiation Facility, respectively. The ^{57}Fe Mössbauer spectra were recorded using a Topologic 500A spectrometer with a proportional counter described elsewhere[S2]. $^{57}Co(Rh)$

moving in a constant acceleration mode was used as the radioactive source. The Doppler velocity of the spectrometer was calibrated with respect to α-Fe. Samples were protected under Ar atmosphere during Mössbauer measurements. Self-made Fe_2N was prepared as reference material from nitridation of granular Fe_2O_3 in NH_3 by the temperature-programmed reaction method according to literature[S3]. The synthesized Fe_2N was examined by XRD. Solid state ^{11}B MAS NMR experiments were carried out at room temperature on a Bruker AVANCE 500 MHz (11.7 T) spectrometer at a frequency of 128.3 MHz. The chemical shifts are referenced to BF_3OEt_2 at 0 ppm for ^{11}B nuclei. FTIR measurements were performed on a Varian 3100 unit. Raman spectra were obtained in a RENISHAW inVia Raman Microscope. The ratio of H_2 and N_2 was determined by a SHIMADZU GC-2014C gas chromatography. Differential scanning calorimeter (DSC) data were obtained from a SETARAM C80 thermal analysis system equipped with a closed sample cell.

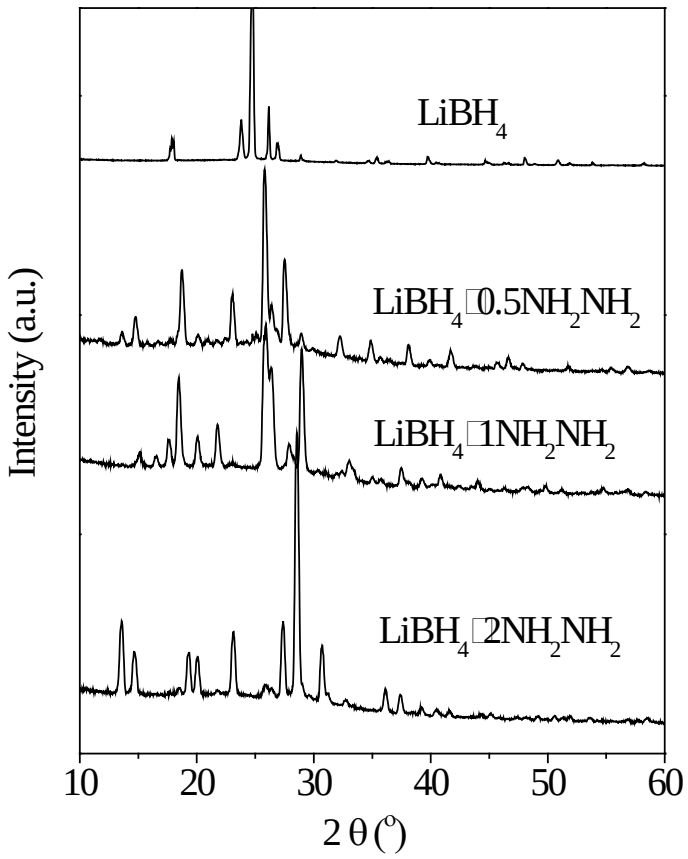

Figure S1. XRD patterns of $LiBH_4$ complexed with hydrazine in different molar ratios.

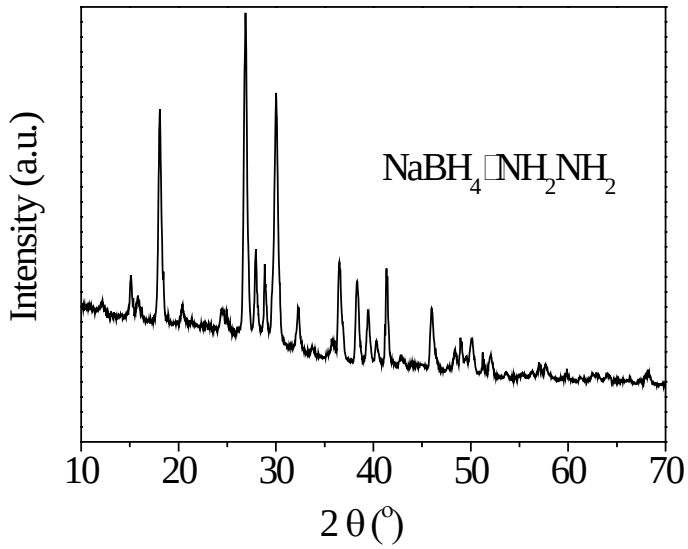

Figure S2. XRD patterns of $NaBH_4$ complexed with hydrazine in a molar ratio of 1:1.

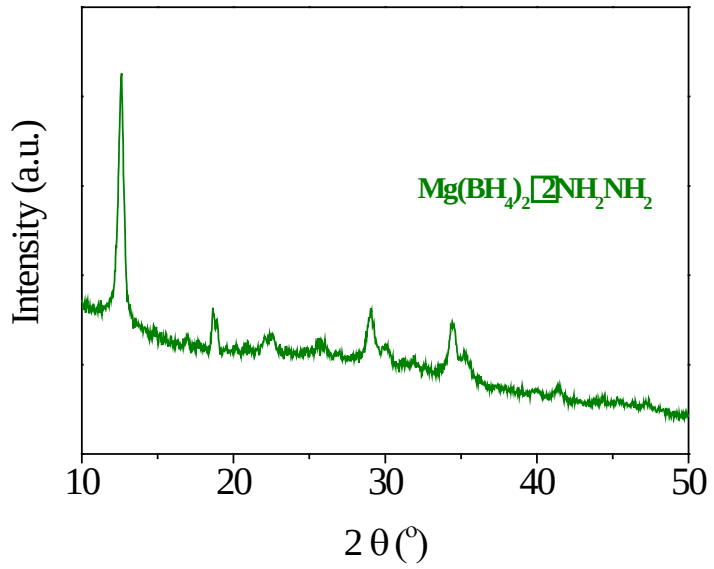

Figure S3. XRD patterns of $Mg(BH_4)_2$ complexed with hydrazine in a molar ratio of 1:2.

In all the cases, phases of pristine borohydrides were disappeared. Further structural identifications are undergoing for Mg and Na-based hydrazinates.

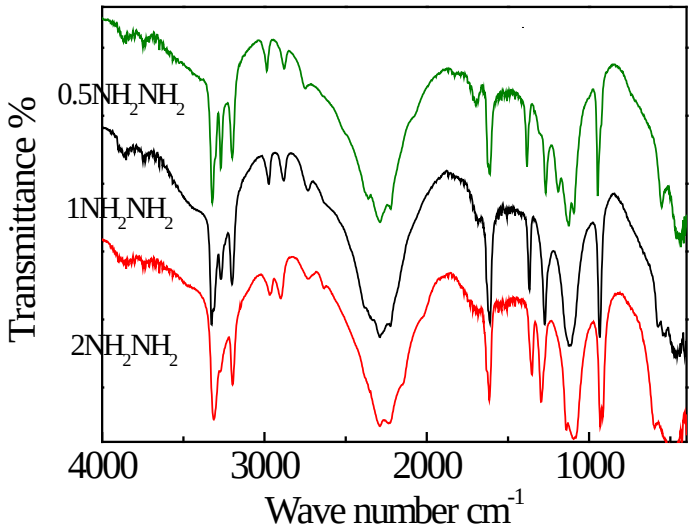

Figure S4. FTIR spectra of $LiBH_4$ complexed with hydrazine of different molar ratios.

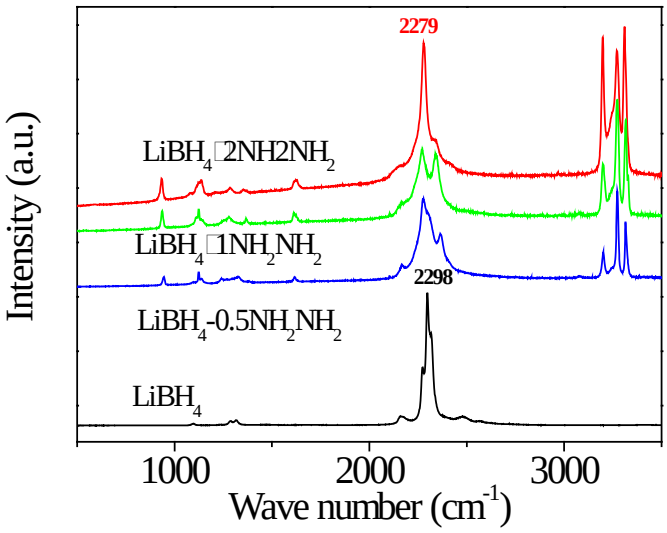

Figure S5. Raman spectra of pristine $LiBH_4$ and $LiBH_4$ complexed with hydrazine.

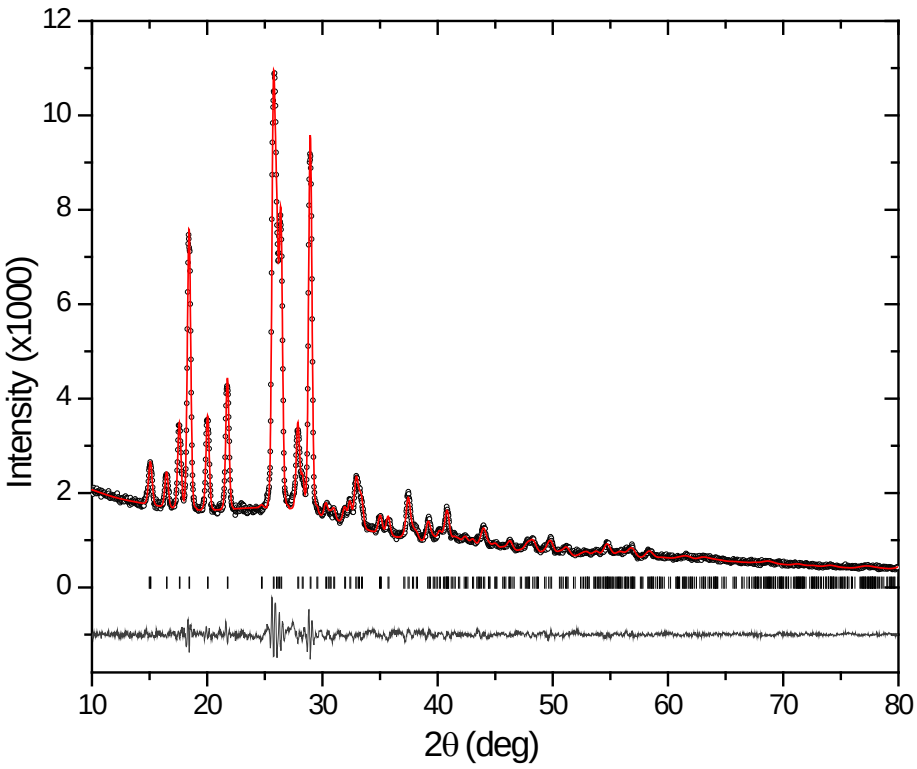

Figure S6. Experimental (circles), fitted (line), and difference (line below observed and calculated patterns) XRD profiles for $LiBH_4 \bullet NH_2NH_2$ at 298 K (Cu Ka radiation). Vertical bars indicate the calculated positions of Bragg peaks.

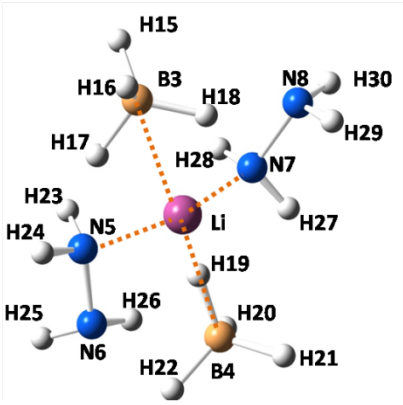

Figure S7. Close contacts around the Li^+ center in $LiBH_4 \bullet NH_2NH_2$

Table S1. Interatomic distances (Å) in crystal structure of $LiBH_4 \bullet NH_2NH_2$ at room temperature

Atoms	Bond distance (Å)	Atoms	Bond distance (Å)
H1···H4	2.323	B3 H15	1.231
H2···H8	2.100	B3 H16	1.225
H3···H6	2.318	B3 H17	1.223
H5···H7	2.323	B3 H18	1.227
H9···H10	2.318	B4 H19	1.217
H11···H12	2.066	B4 H20	1.228
H13···H14	2.066	B4 H21	1.226
Li1 B1	2.322	B4 H22	1.230
Li1 B2	2.437	N5 H23	1.030
Li2 B1	2.600	N5 H24	1.030
Li3 B2	2.334	N6 H25	1.025
Li1 N1	2.427	N6 H26	1.029
Li1 N3	2.131	N7 H27	1.027
Li2 N1	2.140	N7 H28	1.029
Li3 N4	2.215	N8 H29	1.036
N1 N2	1.447	N8 H30	1.031
N3 N4	1.452		

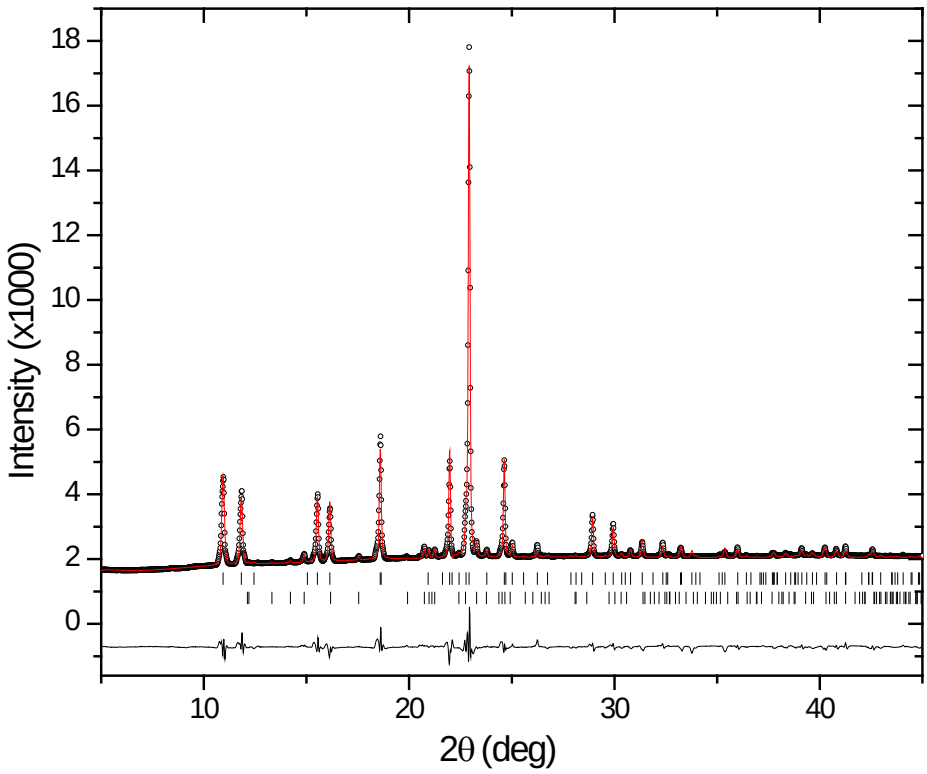

Figure S8. Experimental (circles), fitted (line), and difference (line below observed and calculated patterns) XRD profiles for $LiBH_4 \cdot 2NH_2NH_2$ at 298 K (λ=1.238Å). Pattern also includes a small amount of $LiBH_4 \cdot NH_2NH_2$ phase. Vertical bars indicate the calculated positions of Bragg peaks of $LiBH_4 \cdot 2NH_2NH_2$ and $LiBH_4 \cdot NH_2NH_2$ (from the top).

Table S2. Interatomic distances (Å) in crystal structure of $LiBH_4 \cdot 2NH_2NH_2$ at room temperature

Atoms	Bond distance (Å)	Atoms	Bond distance (Å)
Li1 N1	2.097	N3 N5	1.452
Li1 N2	1.962	N3 H2	1.030
Li1 N3	2.097	H1···H2	2.097
Li1 N4	2.248	H1···H5	1.926
B1 H1	1.231	H3···H4	2.163
B1 H3	1.234	H5···H7	2.397
B1 H6	1.230	H6···H9	1.940
B1 H7	1.225	H7···H8	2.229

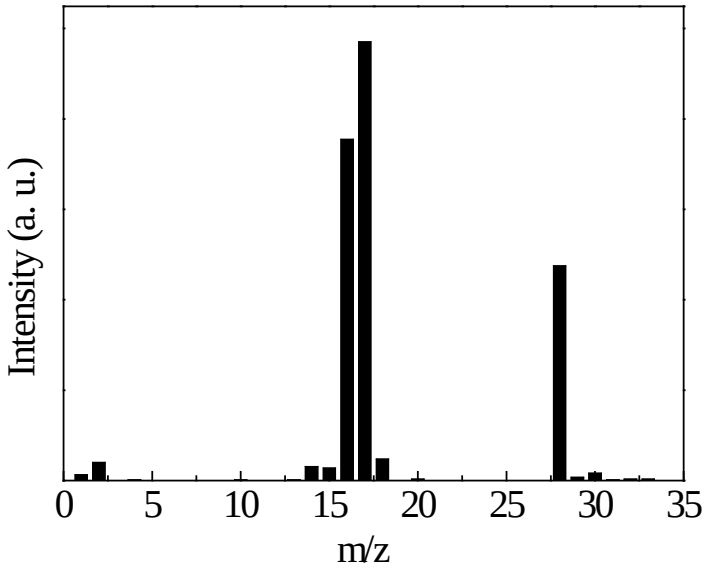

Figure S9. MS Results of gaseous products from volumetric release measurement on neat hydrazine at 140 °C.

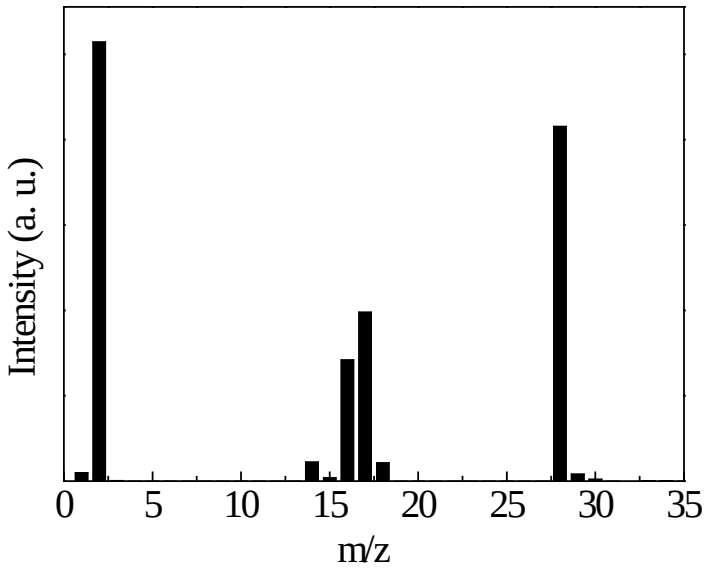

Figure S10. MS Results of gaseous products from volumetric release measurement on $LiBH_4 \bullet 2NH_2NH_2$ at 140 °C.

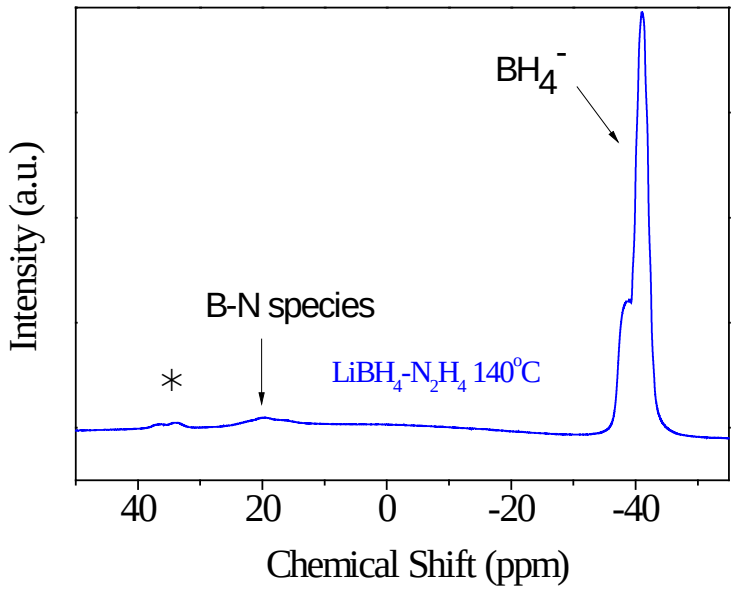

Figure S11. ^{11}B MAS NMR spectrum of solid residue of post-140 °C decomposed $LiBH_4 \bullet NH_2NH_2$.

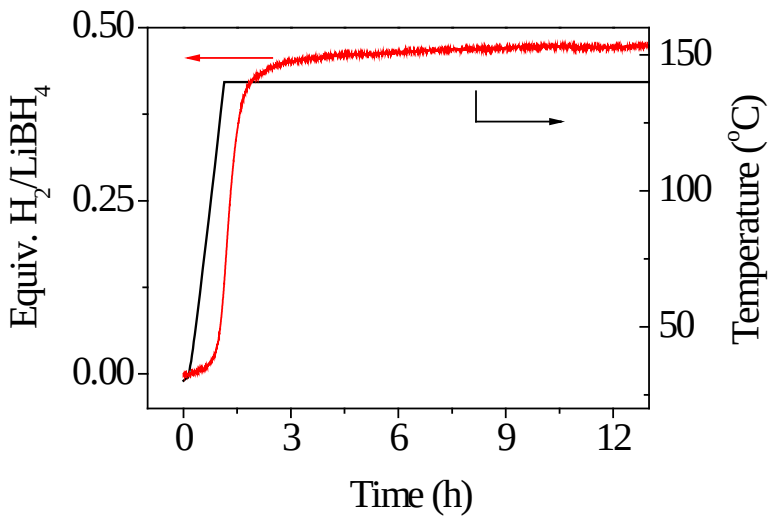

Figure S12. Volumetric release measurement on $LiBH_4 \bullet 1/3NH_2NH_2$ at 140 °C.

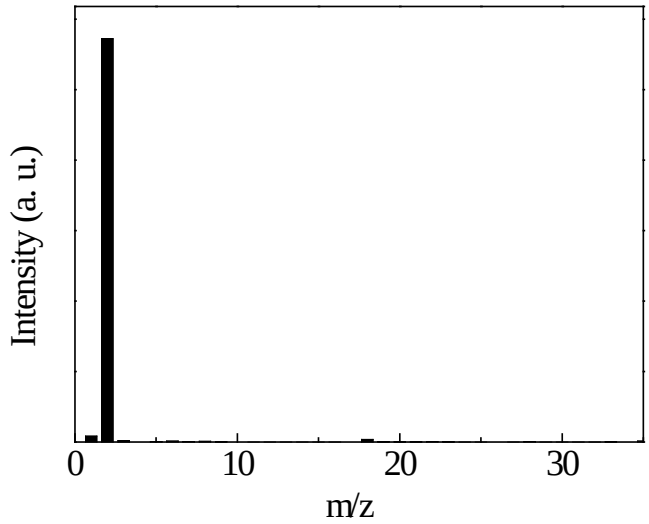

Figure S13. MS results of gaseous products from volumetric release measurement on $LiBH_4$•1/3NH_2NH_2 at 140 °C.

From Figure S11, a weak B-N species can be detected, which suggests the formation of H_2 is derived from the combination of $H^{\delta-}$ (BH_4^-) and $H^{\delta+}$ (NH_2). We would like to point out that direct hydrogen release from $LiBH_4$-NH_3 under the same condition may be ruled out.[S4]

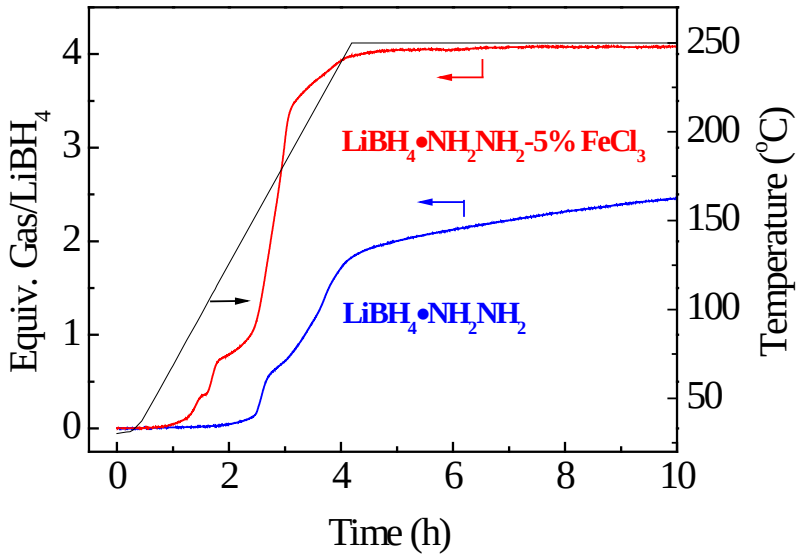

Figure S14. Volumetric release measurements on the neat $LiBH_4$•NH_2NH_2 and the Fe-catalyzed $LiBH_4$•NH_2NH_2 samples at 250 °C.

As hydrazine has certain vapor pressure in the $LiBH_4$ hydrazinates, decomposition of the hydrazinates under a flow of argon will result in the substantial loss of NH_2NH_2 prior to the decomposition. We, therefore, conduct the decomposition in a closed vessel. The DSC measurement on the 2 mol% $FeCl_3$-doped $LiBH_4$•NH_2NH_2 was obtained in a closed cell. Notably, the practical tank for hydrogen production resembles the condition applied here.

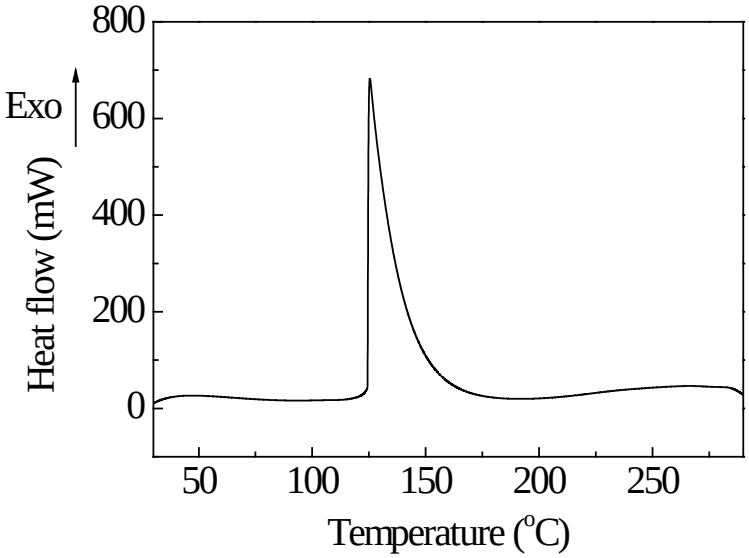

Figure S15. DSC curve of the decomposition of 2 mol% $FeCl_3$-doped $LiBH_4$•NH_2NH_2.

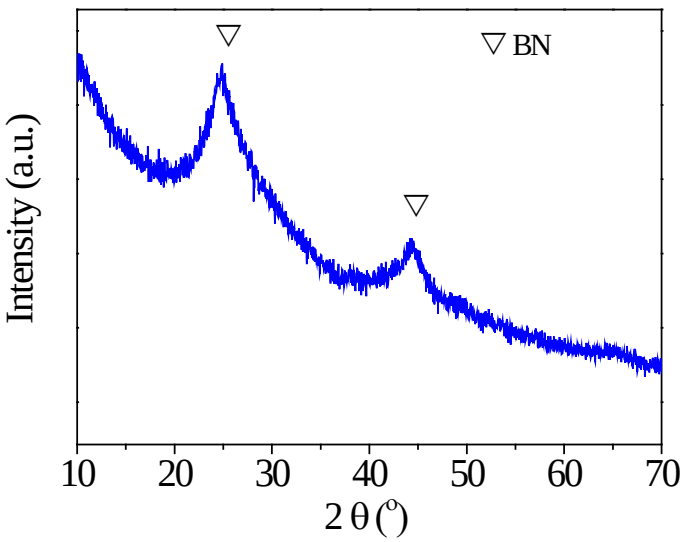

Figure S16. XRD patterns of post-300 °C dehydrogenated Fe-catalyzed $LiBH_4$•NH_2NH_2 sample.

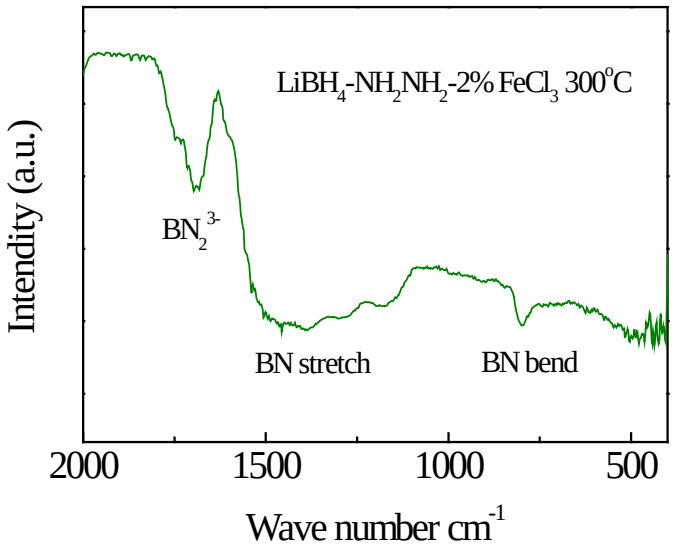

Figure S17. FTIR spectrum of post- 300 °C dehydrogenated Fe-catalyzed $LiBH_4 \bullet NH_2NH_2$ sample.

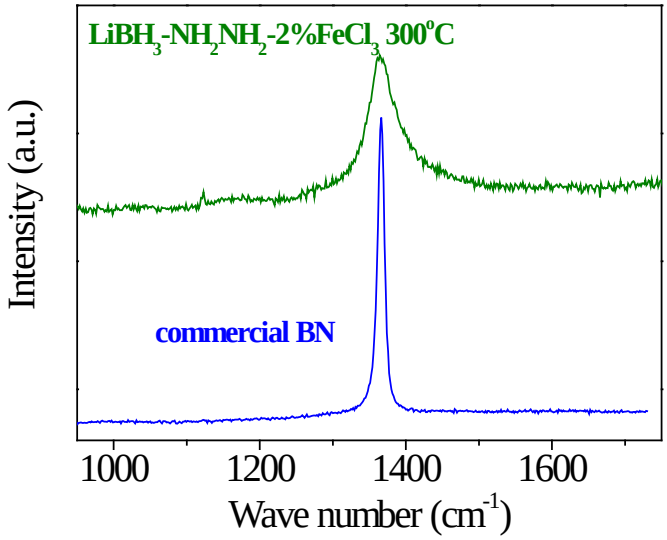

Figure S18. Raman spectra of commercial BN and post-300 °C dehydrogenated Fe-catalyzed $LiBH_4 \bullet NH_2NH_2$ samples.

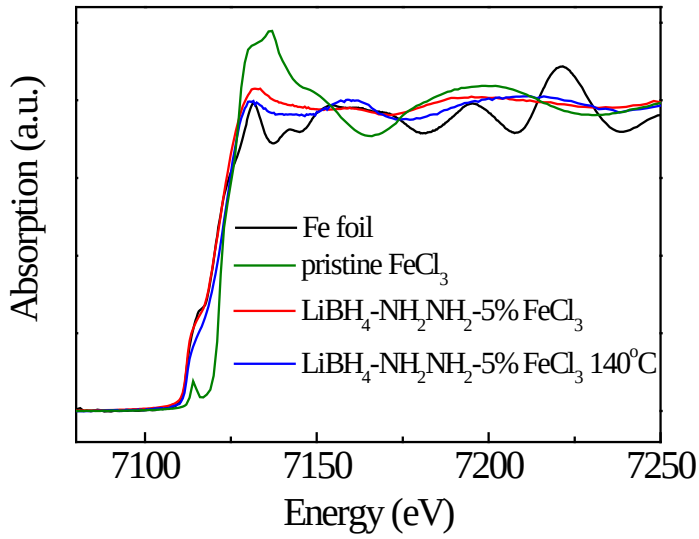

Figure S19. Fe K-edge XANES spectra of Fe foil, pristine $FeCl_3$, 5% $FeCl_3$-doped $LiBH_4$-NH_2NH_2, post-dehydrogenated 5% $FeCl_3$-doped $LiBH_4$•NH_2NH_2.

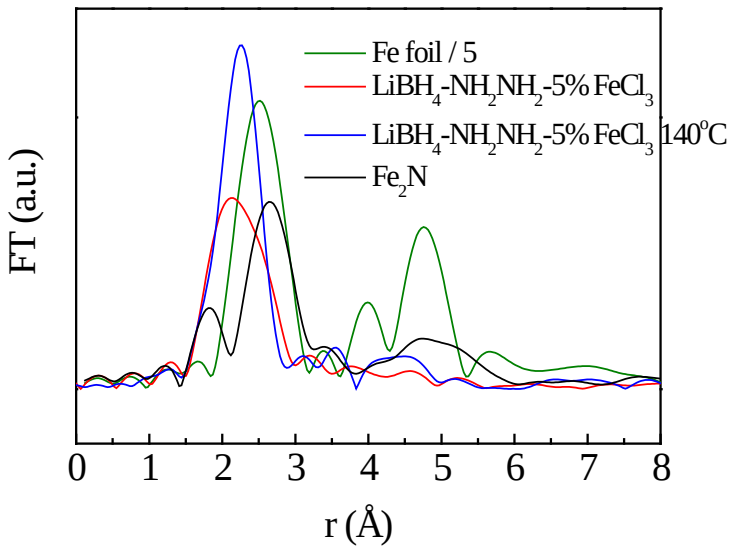

Figure S20. Fourier transform of Fe K-edge EXAFS of Fe foil, 5 mol% $FeCl_3$-doped $LiBH_4$-NH_2NH_2, post-dehydrogenated 5 mol% $FeCl_3$-doped $LiBH_4$-NH_2NH_2 and self-made Fe_2N.

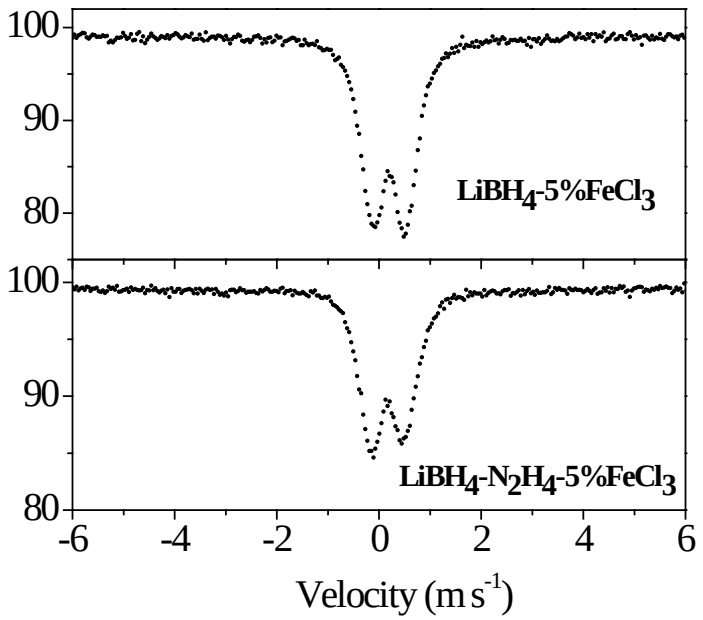

Figure S21. ^{57}Fe Mössbauer spectra of 5.0 mol % $FeCl_3$-doped $LiBH_4$•NH_2NH_2 and 5.0 mol % $FeCl_3$-doped $LiBH_4$.

As illustrated in Figure S19, the Fe K-edge X-ray absorption near edge structure (XANES) spectra of the pre- and post-dehydrogenated $FeCl_3$-doped samples are similar to each other but different from the pristine $FeCl_3$ and resemble to that of Fe foil, indicating that Fe possesses a reduced state in these two samples. However, the Fourier transformed patterns (Figure S20) of these two samples are different from that of Fe foil. In our previous reports, $FeCl_3$ can be reduced by BH_3 group to amorphous Fe-B alloy with a chemical valence close to zero[S1]. It was also reported that ferric or ferrous salts were easy to be reduced by BH_4^- to form amorphous Fe-B alloy[S5]. In this work, the peaks of Fourier transformed spectrum of pre- and post-dehydrogenated samples are close to that of FeB alloy reported[S2] and are different from that of self-made Fe_2N. Thus, we believe that amorphous Fe-B alloy is formed and functions as active center in the dehydrogenation process. The ^{57}Fe Mössbauer spectrum (Figure S21) of 5.0 % $FeCl_3$-doped $LiBH_4$•NH_2NH_2 illustrates an isomer shift (IS) at 0.17 mm s^{-1}, which is close to the IS of $Fe_{44}Co_{19}B_{37}$, $Fe_{62}B_{38}$ and Fe-B alloys in the references.[S1,S2,S5] Moreover, the ^{57}Fe Mössbauer spectrum of $LiBH_4$ ball milled with 5.0 mol % $FeCl_3$ is similar to the 5.0 % $FeCl_3$-doped

$LiBH_4 \bullet NH_2NH_2$ sample, further evidencing the formation of Fe-B alloy (Figure S21 & Table S3).

Table S3. ^{57}Fe Mössbauer parameters of 5 mol % $FeCl_3$-doped $LiBH_4 \bullet NH_2NH_2$ and 5.0 mol % $FeCl_3$-doped $LiBH_4$.

Composition	**Oxidation state of Fe**	**IS[a] (mm s^{-1})**	**QS[b] (mm s^{-1})**	**Spectral area (%)[c]**	**Line-width[d] (mm s^{-1})**
5%$FeCl_3$-dopedLi $BH_4 \bullet NH_2NH_2$	alloy	0.17	0.65	100	0.53
5%$FeCl_3$-$LiBH_4$	alloy	0.20	0.64	100	0.53

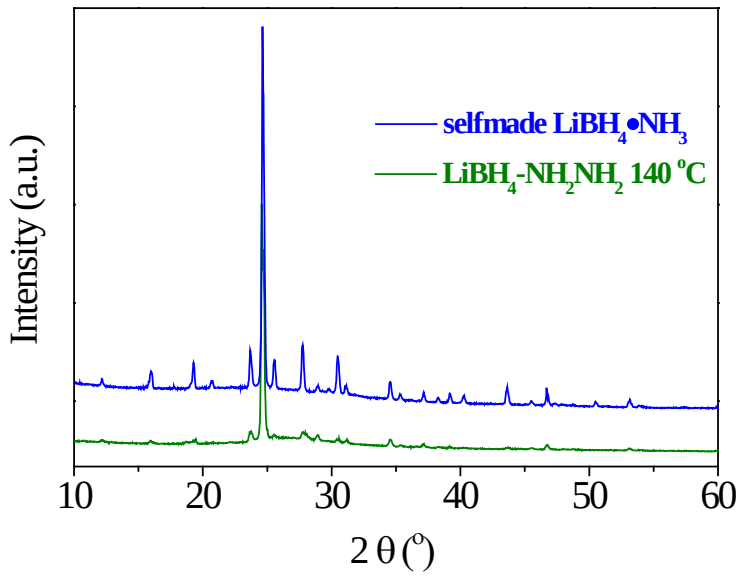

Figure S22. XRD patterns of partially decomposed product of $LiBH_4 \bullet NH_2NH_2$ at 140 °C compared with the self-made $LiBH_4 \bullet NH_3$ sample.

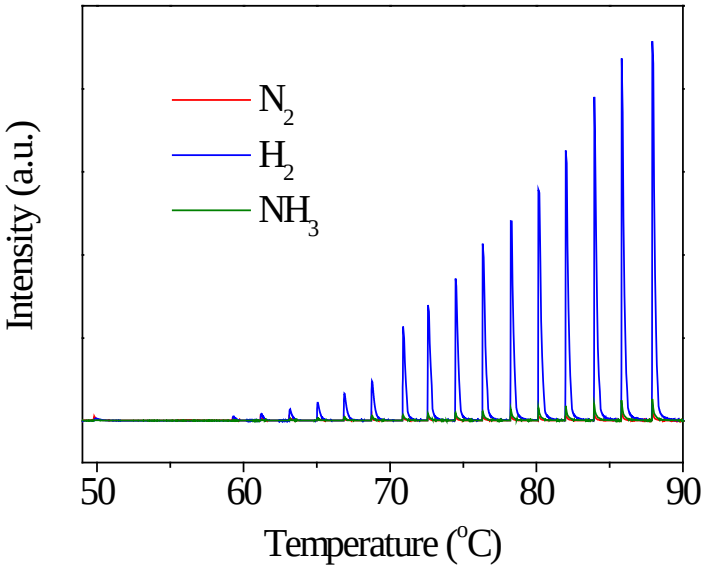

Figure S23. MS profiles of gaseous product from the Fe-catalyzed $LiBH_4 \bullet NH_2NH_2$ sample at elevating temperature.

References

[S1] T. He, J. Wang, G. Wu, H. Kim, T. Proffen, A. Wu, W. Li, T. Liu, Z. Xiong, C. Wu, H. Chu, J. Guo, T. Autrey, T. Zhang, P. Chen, *Chem. Eur. J.* **2010**, *16*, 12814-12817.

[S2] T. He, J. Wang, T. Liu, G. Wu, Z. Xiong, J. Yin, H. Chu, T. Zhang, P. Chen, *Catal. Today* **2011**, *170*, 69-75.

[S3] M. Zheng, X. Chen, R. Cheng, N. Li, J. Sun, X. Wang, T. Zhang, *Catal. Commun.* **2006**, *7*, 187-191.

[S4] a) X. Zheng, G. Wu, W. Li, Z. Xiong, T. He, J. Guo, H. Chen, P. Chen, *Energy Environ. Sci.* **2011**, *4*, 3593-3600; b) Y. Guo, G. Xia, Y. Zhu, L. Gao, X. Yu, *Chem. Commun.* **2010**, *46*, 2599-2601.

[S5] J. van Wonterghem, S. Morup, C. J. W. Koch, S. W. Charles, S. Wells, *Nature* **1986**, *322*, 622-623.